Eur. Phys. J. B **54**, 175–183 (2006)
DOI: 10.1140/epjb/e2006-00433-1

THE EUROPEAN PHYSICAL JOURNAL B

Optical investigation of the metal-insulator transition in $FeSb_2$

A. Perucchi[1], L. Degiorgi[1,a], Rongwei Hu[2,3], C. Petrovic[2], and V.F. Mitrović[3]

[1] Laboratorium für Festkörperphysik, ETH Zürich, 8093 Zürich, Switzerland
[2] Condensed Matter Physics, Brookhaven National Laboratory, Upton NY 11973, USA
[3] Physics Department, Brown University, Providence RI 02912, USA

Received 10 July 2006 / Received in final form 25 August 2006
Published online 8 December 2006 –

Abstract. We present a comprehensive optical study of the narrow gap $FeSb_2$ semiconductor. From the optical reflectivity, measured from the far infrared up to the ultraviolet spectral range, we extract the complete absorption spectrum, represented by the real part $\sigma_1(\omega)$ of the complex optical conductivity. With decreasing temperature below 80 K, we find a progressive depletion of $\sigma_1(\omega)$ below $E_g \sim 300$ cm^{-1}, the semiconducting optical gap. The suppressed (Drude) spectral weight within the gap is transferred at energies $\omega > E_g$ and also partially piles up over a continuum of excitations extending in the spectral range between zero and E_g. Moreover, the interaction of one phonon mode with this continuum leads to an asymmetric phonon shape. Even though several analogies between $FeSb_2$ and FeSi were claimed and a Kondo-insulator scenario was also invoked for both systems, our data on $FeSb_2$ differ in several aspects from those of FeSi. The relevance of our findings with respect to the Kondo insulator description will be addressed.

PACS. 71.27.+a Strongly correlated electron systems; heavy fermions – 71.30.+h Metal-insulator transitions and other electronic transitions – 75.30.Mb Valence fluctuation, Kondo lattice, and heavy-fermion phenomena – 78.20.-e Optical properties of bulk materials and thin films

1 Introduction

$FeSb_2$ represents an interesting case of narrow gap semiconductor, where a band of itinerant electron states originates in the d_{xy} orbitals of the t_{2g} multiplet. The magnetic properties [1,2] of $FeSb_2$ strongly resemble those seen in FeSi (Refs. [3] and [4]). The magnetic susceptibility of $FeSb_2$ shows a diamagnetic to paramagnetic crossover around 100 K (Ref. [1]); however in contrast to FeSi, with a very small low temperature (T) impurity tail in the diamagnetic region. The dc electrical transport ($\rho(T)$) in $FeSb_2$ along the a and c axes is semiconducting ($\rho(T)$ rapidly increases for $T < 100$ K), whereas the b axis exhibits a metal-semiconductor crossover at temperature $T_{cr} \sim 40$–80 K, depending on the current alignment [1].

Aeppli and Fisk [5] proposed that the underlying physics of FeSi share common features with a class of rare earth compounds, known as hybridization gap semiconductors or Kondo insulators. The analogies between FeSi and $FeSb_2$, pointed out above, would suggest that also $FeSb_2$ might belong to the class of d-electron based Kondo insulators. Within the Kondo insulator's scenario, one considers two narrow hybridized bands of width W in the density of states, separated by the gap E_g. At $T = 0$ the electrons populate a lower hybridized band, and with the increase of T the electrons start populating the higher band, resulting in a thermally activated Pauli susceptibility [5]. This approach, successfully applied to FeSi, seems to work out for $FeSb_2$, as well [1,2]. The applicability of the Kondo insulating scenario in FeSi as well as in $FeSb_2$ is of particular interest because of possible relations between theoretical descriptions of d- and f-electron systems.

The absorption spectrum of FeSi was intensively investigated as well [6–11]. At low temperatures, the charge excitation spectrum of FeSi is characterized by a direct gap of about 95 meV. The spectral weight, suppressed by the gap opening, is transferred to high energies. It has been long debated up to which energy the total spectral weight in FeSi is effectively fully recovered [6,7]. In the data of Degiorgi et al. (Ref. [7]), the spectral weight is essentially recovered at a frequency $\omega_c \sim 4E_g$, therefore without any need to invoke an integration of $\sigma_1(\omega)$ to very high frequencies. This conclusion is at variance with claims [6], suggesting a redistribution of spectral weight extending up to very high energies, even beyond the highest energy limit of that experiment. Recent low temperature ellipsometry measurements accurately determine the

[a] e-mail: degiorgi@solid.phys.ethz.ch

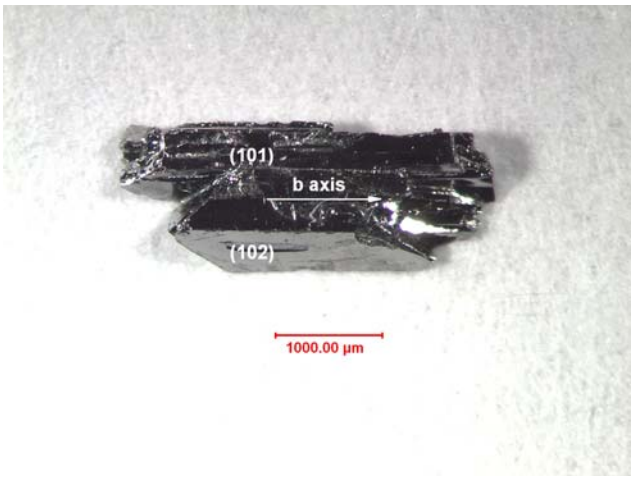

Fig. 1. $FeSb_2$ sample used for our optical investigations. The crystal axes, determined through the Laue spectroscopic experiment, are also shown.

conductivity up to high frequencies [11]. The ellipsometry findings resolved the debate, indicating the redistribution of the spectral weight up to very high frequencies. Moreover, it was found that this feature is indicative of a Kondo insulator description of FeSi (Ref. [6]). For $FeSb_2$ a comprehensive optical study is still missing.

In addition to FeSi, $FeSb_2$ seems to be a promising model system, for investigating the applicability of the Kondo insulator concept versus the nearly itinerant magnetic semiconductor picture for $3d$ intermetallic compounds [12,13]. The absorption spectrum of $FeSb_2$ can reveal important information about its intrinsic physical properties and allow to extract the phonon spectrum as well as the relevant energy scales, like the hybridization gap. To test the applicability of the Kondo insulating concept, it is of interest to investigate the redistribution of spectral weight above and below T_{cr} in $FeSb_2$, addressing the issue of its conservation.

We report on our optical investigation on $FeSb_2$. The paper is organized as follows: we will first characterize the specimen and describe the experiment, followed by the presentation of the optical data. The discussion will first tackle the analysis of the phonon spectrum. Particular attention will be then devoted to the issue of the spectral weight distribution. The relevance of the Kondo insulator scenario for the description of the metal-insulator crossover at T_{cr} in $FeSb_2$ will be emphasized.

2 Experiment and results

Single crystals of $FeSb_2$ are grown from excess Sb flux, as described in reference [1]. The crystals are cut in a rectangular shape with the long direction corresponding to the b crystalline axis. Our sample is shown in Figure 1, which also displays the crystal orientations. We measured the optical reflectivity $R(\omega)$ of our $FeSb_2$ specimen, over a broad spectral range (30 to 10^5 cm^{-1}) and as a function of temperature. The large spectral range is covered with a combination of spectrometers: the far and mid-infrared range were measured with a Fourier spectrometer, based on a Michelson interferometer, and using a He-cooled Bolometer as detector. The visible and ultra violet spectral range were investigated with an home-made Zeiss monochromator set up and a McPherson spectrometer, respectively [7]. Light was polarized along the b axis ($E \parallel b$) and along the direction perpendicular ($E \perp b$) to the b axis within the (102) surface (Fig. 1). The real part $\sigma_1(\omega)$ of the optical conductivity was obtained through Kramers-Kronig (KK) transformation [14,15] of $R(\omega)$. To this end, we applied standard high-frequency extrapolations $R(\omega) \sim \omega^{-s}$ (with

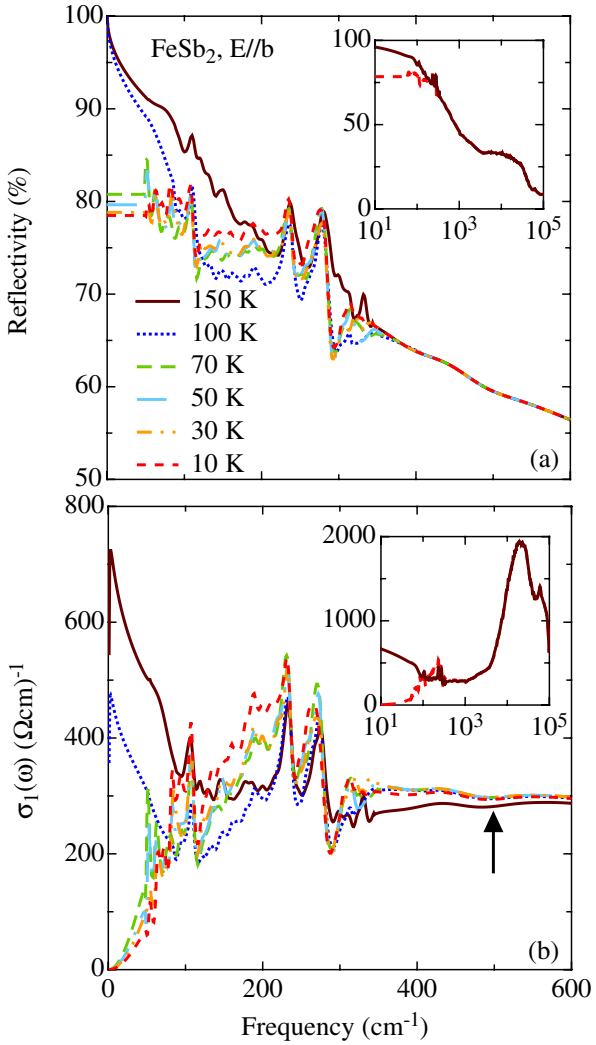

Fig. 2. (Color online) (a) Optical reflectivity $R(\omega)$ and (b) real part $\sigma_1(\omega)$ of the optical conductivity as a function of temperature of $FeSb_2$ in the infrared range, with light polarized along the b crystallographic axis ($E \parallel b$). The arrow indicates the onset of the temperature independent tail, ascribed to the incoherent electronic contribution. Insets: $R(\omega)$ and $\sigma_1(\omega)$ at 10 and 150 K for frequencies up to 10^5 cm^{-1} (the reader should note the use of the logarithmic energy scale).

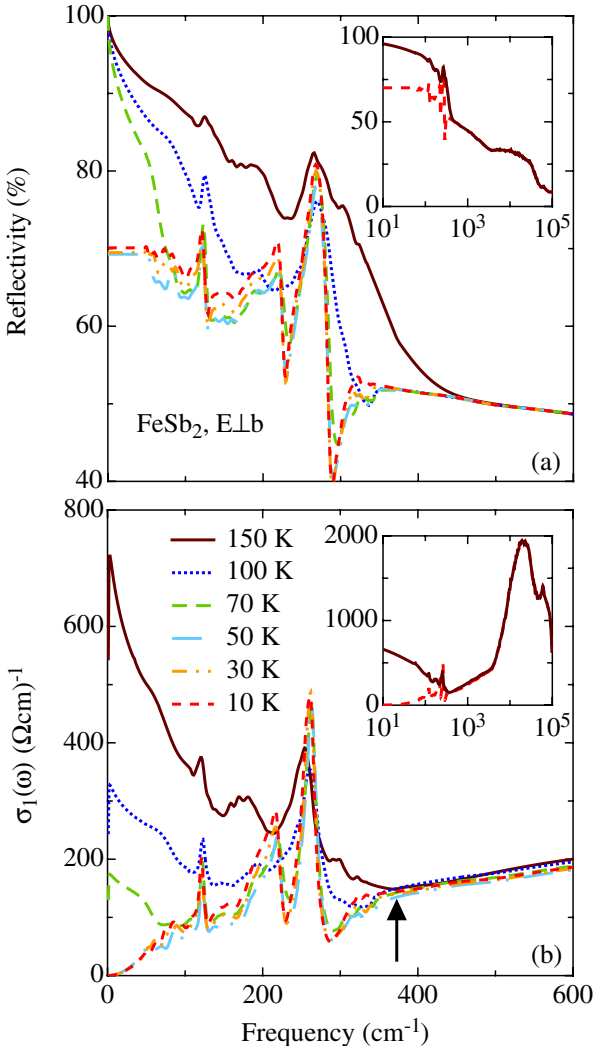

Fig. 3. (Color online) (a) Optical reflectivity $R(\omega)$ and (b) real part $\sigma_1(\omega)$ of the optical conductivity as a function of temperature of $FeSb_2$ in the infrared range, with light polarized perpendicular to the b crystallographic axis ($E \perp b$). The arrow indicates the onset of the temperature independent tail, ascribed to the incoherent electronic contribution. Insets: $R(\omega)$ and $\sigma_1(\omega)$ at 10 and 150 K for frequencies up to 10^5 cm^{-1} (the reader should note the use of the logarithmic energy scale).

$2 < s < 4$) in order to extend the data set above 10^5 cm^{-1} into the electronic continuum. Below 30 cm^{-1}, $R(\omega)$ was extrapolated towards zero frequency either by using the Hagen-Rubens (HR) law $R(\omega) = 1 - 2\sqrt{(\omega/\sigma_{dc})}$ for reflectivity data at $T > T_{cr}$, displaying a metallic behavior, or by imposing $R(\omega < \omega_{min}) = R(\omega_{min} = 30\ \text{cm}^{-1})$ for data in the insulating state at $T < T_{cr}$. The *dc* conductivity values (σ_{dc}) in HR are in fair agreement with the transport results [1]. This is particularly true for $E \perp b$. For $E \parallel b$, the *dc* transport data [1] display between 40 and 70 K a shallow minimum in $\rho(T)$, thus implying a metallic behaviour down to 40 K (Fig. 3 of Ref. [1]). However, it has been shown in reference [1] that deliberate current misalignment in the *ab* plane has substantial influence in the *dc* transport. The minimum in $\rho(T)$ shifts to higher temperatures and the resistivity remarkably increases (Fig. 4 of Ref. [1]). $R(\omega)$ at 50 and 70 K at $\omega \sim 30$ cm^{-1} is lower than the expected value calculated from the HR extrapolation with the $\rho_{dc}(T)$ data [1] and displays a quite flat and insulating-like behaviour below 200 cm^{-1}. The insulating $R(\omega)$ spectra between 40 and 70 K could than be due to the projection of other axes into the electrodynamic response along the b direction. The overall behaviour of $\sigma_1(\omega)$ in the spectral range pertinent to this work is not affected by these low frequency extrapolations [16]. Details pertaining to the experiment, as well as to the analysis of the data, can be found in references [14] and [15].

Figures 2 and 3 present the temperature dependence of $R(\omega)$ and $\sigma_1(\omega)$ in the far-infrared (FIR) spectral range for both polarizations of light, while the insets display the spectra at 10 and 150 K for both quantities over the whole measured spectral range (the reader should pay attention to the use of the logarithmic energy scale in the insets). Above 150 K we did not find any remarkable T-dependence of the optical spectra. $R(\omega)$ at 150 K displays a metallic behavior for both polarization directions, with a plasma edge onset at ∼3000 cm^{-1} (inset of Figs. 2a and 3a). The anisotropy in $R(\omega)$ is not very pronounced at 150 K, even though the $E \perp b$ reflectivity is depleted with respect to $R(\omega)$ along the b axis in the spectral range between 300 and 1000 cm^{-1}. With decreasing T and for both polarizations, $R(\omega)$ flattens in the far infrared range (Figs. 2a and 3a), an indication of a metal to insulator (MI) crossover. The enhancement of phonon-like structures, especially for $E \perp b$, is observed at 10 K (i.e., in the insulating state). $R(\omega)$ at 150 and 10 K merge together at ∼350 and 450 cm^{-1} for light polarization $E \parallel b$ and $E \perp b$, respectively. The anisotropic behavior in the optical response between the two polarization directions becomes more evident at low temperatures. In the far infrared range, $R(\omega)$ at 10 K along the b axis is approximately 10% higher compared to the other crystallographic axis. Furthermore, the anisotropic electrodynamic response is clearly represented by the presence of different phonon features along the two crystallographic directions.

The real part $\sigma_1(\omega)$ of the optical conductivity, as extracted from the KK transformations, is shown in Figures 2b and 3b. At 150 K, one can easily recognize the presence of a Drude metallic term [17] at low frequencies, for both polarization directions, as well as the strong absorption at ∼20 000 cm^{-1} due to an electronic interband transition (inset of Figs. 2b and 3b). With decreasing temperature, the Drude term vanishes along both directions (main panel of Figs. 2b and 3b). Figure 4 displays $\sigma_1(\omega)$ in the far infrared spectral range at two selected temperatures for both polarizations. For $E \parallel b$ we can clearly distinguish phonon modes at ∼106, 231, 270 cm^{-1} (arrows in Fig. 4a); the latter one seems to be made up by two distinct modes, yet not completely resolved (i.e., at approximately 257 and 271 cm^{-1}). On the other hand, $\sigma_1(\omega)$ for $E \perp b$ displays phonon features at ∼121, 216, 261 cm^{-1} (arrows in Fig. 4b). The mode at 216 cm^{-1} is clearly present at low temperatures only.

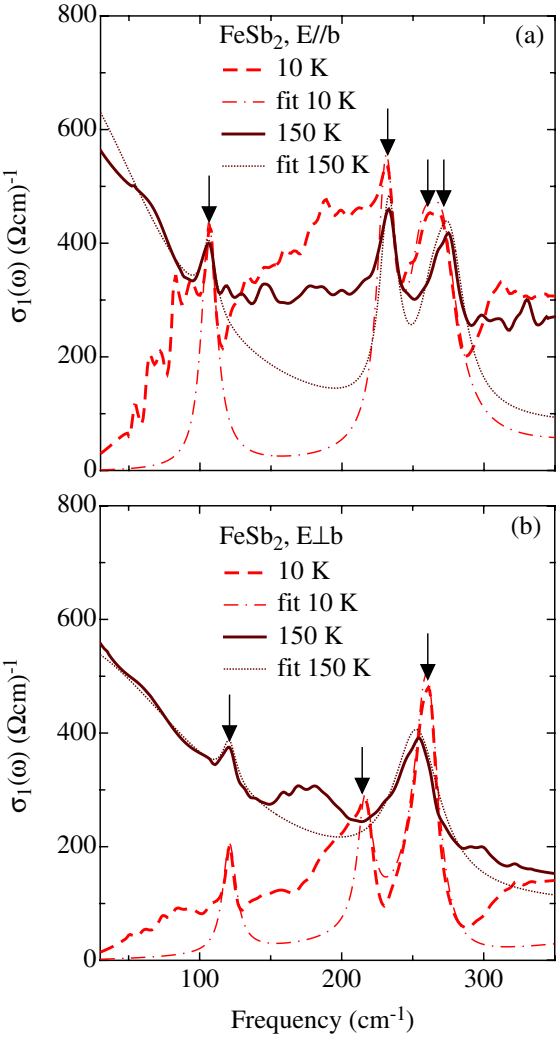

Fig. 4. (Color online) Real part $\sigma_1(\omega)$ of the optical conductivity at 10 and 150 K of $FeSb_2$ in the far infrared range (30–350 cm^{-1}), with light polarized along (a) and perpendicular (b) to the b crystallographic axis. The Lorentz (Fano)-Drude fit (see text) for both temperatures is shown. The arrows indicate the phonon modes for which a Lorentz (Fano) oscillator was assigned.

3 Discussion

3.1 The fitting procedure

The optical conductivity is analyzed within the framework of the phenomenological Lorentz-Drude [14,15] model extended to the Fano approach [18–20] in order to account for the asymmetric shape in the phonon modes. The Drude metallic behavior is defined by the formula:

$$\sigma_D(\omega) = \frac{\omega_{pD}^2}{4\pi\gamma_D}\frac{1}{1-i\omega/\gamma_D}, \qquad (1)$$

where the plasma frequency is $\omega_{pD} = \sqrt{4\pi Ne^2/m}$ and γ_D is the scattering rate. Besides the Drude term, we add four and two Lorentz harmonic oscillators for $E \parallel b$ and $E \perp b$, respectively. The contribution due to a Lorentz harmonic oscillator is:

$$\sigma^j_{\text{Lorentz}}(\omega) = \frac{\omega_{pj}^2}{4\pi}\frac{\omega}{i(\omega_{0j}^2-\omega^2)+\omega\gamma_j}, \qquad (2)$$

where ω_{0j} is the resonance frequency, γ_j the damping and ω_{pj} the strength of the j-mode. For $E \perp b$, there is additionally a third contribution, described by a Fano lineshape for the asymmetric mode at 261 cm^{-1}. The contribution due to the Fano mode is given by the equation [19,20]:

$$\sigma^j_{\text{Fano}}(\omega) = i\sigma_{0j}\frac{(q_j+i)^2}{x_j(\omega)+i}, \qquad (3)$$

with

$$x_j(\omega) = \frac{\omega_{0j}^2-\omega^2}{\gamma_j\omega}, \text{ and } \sigma_{0j} = \frac{\omega_{pj}^2}{\gamma_j q_j^2}, \qquad (4)$$

where the same notation as in equation (2) has been used. The dimensionless q_j Fano parameter is a measure of the degree of asymmetry of the peak at ω_{0j} (for $|q| \to \infty$ a Lorentzian lineshape is recovered). The Lorentz and Fano contributions describe the modes, marked by arrows in Figure 4, which clearly develop at low temperatures.

Tables 1 and 2 summarize the temperature dependence of the parameters employed in our fits. We observe that with decreasing temperature, the weight of the Drude term in the fit decreases for both polarizations. From our fits we can define two intervals of temperatures for the MI crossover, $T_{MI}^{\parallel b}$ = 70–100 K and $T_{MI}^{\perp b}$ = 50–70 K, as the range of temperatures at which the Drude term vanishes. Our T_{MI} values are in fair agreement with T_{cr}, which defines the metal-semiconducting crossover in the $\rho(T)$ transport data [1,21]. Another interesting aspect in the infrared spectra of $FeSb_2$ is the quite large mode strength of the infrared active phonons. Particularly, the phonons at ω_{02}, ω_{03} and ω_{04} for $E \parallel b$ and the Fano mode at ω_{03} for $E \perp b$ exhibit at low temperatures mode strengths between 600 and 800 cm^{-1}. In this respect, $FeSb_2$ shares a common property with FeSi (Ref. [6]). Schlesinger et al. also pointed out that strong phonons have been observed in prototype heavy fermions systems and cuprates, as well [6].

While the temperature dependence of the phonon modes and in general of $\sigma_1(\omega)$ in the far infrared (FIR) spectral range will be extensively discussed below, we anticipate here that the proposed fit only partially reproduces the measured spectra (Fig. 4). Indeed, besides the additional Drude component for the effective metallic contribution in $\sigma_1(\omega)$, no attempts have been made to fill the missing part of $\sigma_1(\omega)$ in the far infrared range beyond the clearly detected phonon modes. There is a broad continuum of low frequency excitations in the FIR spectral range and at low temperatures for both polarizations, which is not encountered by this fit procedure.

Table 1. $FeSb_2$ – $E \parallel b$. Lorentz-Drude fit parameters. All parameters are given in units of [cm^{-1}], with the exception of ϵ_∞ which is unit-less.

Parameters	10 K	30 K	50 K	70 K	100 K	150 K
$\boldsymbol{\epsilon_\infty}$	1	1	1	1	1	1
$\boldsymbol{\omega_{pD}}$	–	–	–	–	1400	1900
$\boldsymbol{\gamma_D}$	–	–	–	–	75	85
$\boldsymbol{\omega_{p1}}$	580	510	480	480	300	300
$\boldsymbol{\omega_{01}}$	106.4	107.5	107.5	107.5	107.5	106.3
$\boldsymbol{\gamma_1}$	13	12	10.5	10.5	10.5	12
$\boldsymbol{\omega_{p2}}$	650	650	650	680	590	560
$\boldsymbol{\omega_{02}}$	231	231	231	231	232	232.9
$\boldsymbol{\gamma_2}$	15	15.5	15.5	15.5	15.5	15
$\boldsymbol{\omega_{p3}}$	635	600	615	520	520	455
$\boldsymbol{\omega_{03}}$	257	257	256.5	258.3	258.3	264
$\boldsymbol{\gamma_3}$	25	25	25	25	25	25
$\boldsymbol{\omega_{p4}}$	655	655	650	715	630	625
$\boldsymbol{\omega_{04}}$	271	272.5	273	272	274	276
$\boldsymbol{\gamma_4}$	25	23	20	22	22	25

Table 2. $FeSb_2$ – $E \perp b$. Lorentz-Drude and Fano fit parameters. All parameters are given in units of [cm^{-1}], with the exception of ϵ_∞ and q which are unit-less.

Parameters	10 K	30 K	50 K	70 K	100 K	150 K
$\boldsymbol{\epsilon_\infty}$	1	1	1	1	1	1
$\boldsymbol{\omega_{pD}}$	–	–	–	900	1484.5	2100
$\boldsymbol{\gamma_D}$	–	–	–	80	112.8	130
$\boldsymbol{\omega_{p1}}$	365	350	335	275	225	230
$\boldsymbol{\omega_{01}}$	121	121	122.5	122	123	121
$\boldsymbol{\gamma_1}$	11.5	12	12	9	10	12
$\boldsymbol{\omega_{p2}}$	420	410	400	420	–	–
$\boldsymbol{\omega_{02}}$	216	217	219	219.5	–	–
$\boldsymbol{\gamma_2}$	13	13	13	18	–	–
$\boldsymbol{\omega_{p3}}$	776.1	746.3	724.4	722.6	777	800
$\boldsymbol{\omega_{03}}$	261.4	262.5	263.8	263.4	261.4	254.0
$\boldsymbol{\gamma_3}$	21.1	19.5	19.6	20.3	33.0	40.0
$\boldsymbol{q_3}$	−6.41	−6.87	−7.67	−7.91	−16	−16

3.2 Lattice dynamics

3.2.1 Factor group analysis

$FeSb_2$ crystallizes in the marcasyte-type structure with two formula units per unit cell. $FeSb_2$ is made up of $FeSb_6$ octahedra which form edge sharing chains along the c axis. The space group is the centrosymmetric $Pnnm$ orthorhombic group [1], for which we report the factor group analysis in Table 3. By using the correlation method [22], and after subtracting the acoustic modes, we find for the total irreducible representations:

$$\Gamma_{Pnnm} = 2A_g + 2A_u + 2B_{1g} + B_{1u} + B_{2g} + 3B_{2u} + B_{3g} + 3B_{3u}. \quad (5)$$

Table 3. Normal modes analysis of $FeSb_2$ for the $Pnnm$ symmetry group.

Normal modes	Number of modes Total	Acoustic	Optical	Raman	IR
A_g	2		2	aa, bb, cc	
B_{1g}	2		2	ab	
B_{2g}	1		1	ac	
B_{3g}	1		1	bc	
A_u	2		2		
B_{1u}	2	1	1		E//c
B_{2u}	4	1	3		E//b
B_{3u}	4	1	3		E//a

By comparing our data with the factor group analysis for the number of infrared active phonon modes along the b axis direction ($E \parallel b$), one can notice that our optical measurement suggests the presence of four instead of three phonon modes. Nevertheless, the resonance frequencies of the modes at 257 and 271 cm^{-1} are quite close to each other. Therefore, optical spectra may reveal a slightly lower symmetry for $FeSb_2$ compared to the one predicted by the $Pnnm$ group [1].

Along the direction perpendicular to the b axis ($E \perp b$) three phonon modes are present at low temperature, while only two of them are still observable above 70 K (Ref. [23]). The disappearance of the phonon mode at 216 cm^{-1} above 70 K might suggest that this specific phonon is silent and not anymore infrared active at high temperatures. Nevertheless, no structural changes have been found so far in $FeSb_2$ down to 10 K (see Figs. 2b and 2c in Ref. [2]). However, there is a change in the bond distances, which get somewhat shorter on cooling below 75–100 K. Interestingly the crossover temperature T_{cr} coincides with the temperature region of maximum distortion in the Fe–Sb–Fe angle [2].

3.2.2 Fano analysis

A blow up of the spectral range pertinent to the asymmetric mode at 261 cm^{-1} for $E \perp b$ at 10 K is displayed in Figure 5a. It is easily recognized that the Fano mode is more appropriate than a simple Lorentz oscillator in order to reproduce the overall shape of this mode. The temperature dependence of the fitting parameters for this peculiar mode is displayed in Figures 5b–5e. Furthermore, there seems to be a clear correlation between the overall temperature dependence of all parameters describing the mode at 261 cm^{-1} and the MI crossover at $T_{MI}^{\perp b}$ (dashed lines in Figs. 5b–5e). We point out that the temperature dependence of the fit parameters (particularly of ω_{p3} and ω_{03}) displays around $T_{MI}^{\perp b}$ a broad minimum and maximum, respectively (Ref. [21]). The oscillator strength is associated to the effective transverse charge and has a non-trivial temperature dependence (Fig. 5b) since it first decreases with increasing T, passes through the minimum between 50 and 70 K and then increases again.

A similar trend is also found for the resonance frequency ω_{03} (Fig. 5c), which slowly increases with

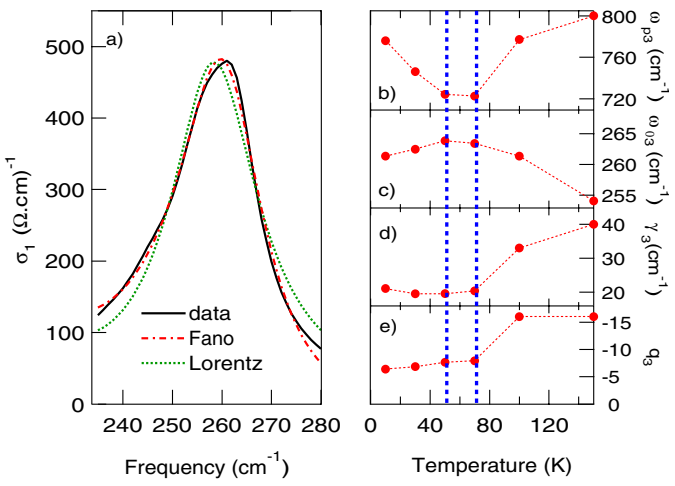

Fig. 5. (Color online) (a) Blow-up of $\sigma_1(\omega)$ around the mode at 261 cm^{-1} at 10 K and for $E \perp b$. The fits of this mode with either a Lorentz harmonic oscillator or a Fano lineshape are shown for comparison. (b) Temperature dependence of the oscillator strength ω_{p3}, (c) resonance frequency ω_{03}, (d) scattering rate γ_3, and (e) asymmetry factor q_3 of the mode at 261 cm^{-1} within the Fano-like fit. The blue dashed lines indicate the lower and upper limits of $T_{MI}^{\perp b}$, respectively.

increasing T before displaying a well defined softening at high temperatures. As already anticipated above, X-ray diffraction studies [2] have established that the Fe–Sb–Fe bond angle, associated with the edge sharing octahedra along the c axis, increases above 100 K. The T-dependence of the Fe–Sb–Fe angle is rather similar to the behavior of ω_{03}.

The damping factor γ_3 (Fig. 5d) increases above $T_{MI}^{\perp b}$. Since $\gamma \sim 1/\tau$, this indicates a two times higher phonon lifetime τ in the low T insulating state. Such a strong correlation between the onset of the insulating state and the loss of phononic relaxational channels also suggests the presence of a coupling mechanism between the electronic degrees of freedom and the lattice vibrations, as already claimed for FeSi (Ref. [24]).

Finally, Figure 5e displays the T-dependence of the dimensionless Fano parameter q. At high T, $|q|$ is of the order of 16. Such a high q-value implies that above 100 K an asymmetric phonon lineshape can be hardly recognized; a Lorentz harmonic oscillator would fit equally well this mode. On the other hand, q takes values between –6.4 and –7.9 below $T_{MI}^{\perp b}$, indicating a sizable asymmetric lineshape. The presence of Fano lineshapes is predicted when a discrete lattice vibration is degenerate with states belonging to a continuum which may be of electronic or magnetic nature [18]. Interestingly, Fano lineshapes have been also observed in the infrared spectra of FeSi (Ref. [24]). In that case, the asymmetry was ascribed to the interaction of the phonon mode with an electronic resonance peaked in the mid-infrared range, i.e., above the phonon resonance frequency. However, for $FeSb_2$ the sign of q (<0) is consistent with the picture of the phonon at ∼261 cm^{-1} coupled to an energy scale which is lower than the phonon resonance frequency. The forthcoming analysis of the spectral weight distribution in the absorption spectrum of $FeSb_2$ will shed more light on this low energy scale.

3.3 Spectral weight analysis

The $\sigma_1(\omega)$ spectrum at 10 K presents a clear depletion below about 350 cm^{-1} for the $E \perp b$ direction (Fig. 3b and its inset). This depletion coincides with the onset of a broad and temperature independent tail, ascribed to the incoherent electronic contribution (arrow in Fig. 3b). Along the $E \parallel b$ direction the phonon modes overcast the onset for such a depletion of $\sigma_1(\omega)$. However, it is safe to say that the depletion of $\sigma_1(\omega)$ develops in the spectral range between 100 and 450 cm^{-1} (Fig. 2 and inset Fig. 2b). Below 100 cm^{-1} the depletion of weight gets more pronounced. Above 450 cm^{-1} all spectra merge together in the low frequency tail of the incoherent electronic contribution (arrow in Fig. 2b). We call such an energy, where the depletion in $\sigma_1(\omega)$ occurs, E_g. This is an appropriate estimation for the insulating optical gap in $FeSb_2$. The value of E_g is comparable or slightly larger than its estimation based on the activated behaviour of the resistivity, which indicates $\Delta_\rho(a,c)$ ∼200 cm^{-1}, and $\Delta_\rho(b)$ ∼170 cm^{-1} (Ref. [1]). Similarly to the case of FeSi (Ref. [9]), discrepancies in the gap value among different experiments could be reconciled by assuming a small indirect energy gap for the transport properties and a larger direct gap for the optical response. The gap fills in progressively upon increasing the temperature, while a temperature dependence of the gap edge, as observed in FeSi (Ref. [24]), cannot be clearly recognized in $FeSb_2$. E_g (i.e., the depletion of $\sigma_1(\omega)$) is not observable above the MI crossover temperature.

By integrating the optical conductivity (i.e., $\int_0^{\omega_c} \sigma_1(\omega)d\omega$), we can achieve the spectral weight encountered in the absorption spectrum over a frequency interval between zero and ω_c. Because of the temperature dependence of $\sigma_1(\omega)$ (Figs. 2 and 3), there is an obvious redistribution of the spectral weight from low to high frequencies in our spectra. A sum rule [14,15] requires that the integrated area under $\sigma_1(\omega)$ must be unchanged at any temperature; therefore predicting the conservation of the spectral weight. In a conventional semiconducting scenario, the T-induced MI transition is simply due to the thermal excitation of charge carriers through the energy gap E_g. From an optical point of view, one would therefore expect that by lowering the temperature through $T_g = E_g/k_B$ the Drude term progressively vanishes while the spectral weight lost at $\omega < E_g$ redistributes just above and close to E_g. Such a picture is inadequate for $FeSb_2$. Figure 6 displays the temperature dependence of the integrated spectral weight up to about 10 eV and for both polarization directions. One can observe the clear depletion of spectral weight for temperature below T_{MI} (as defined before). Such a depletion of weight is particularly pronounced below an energy scale of about

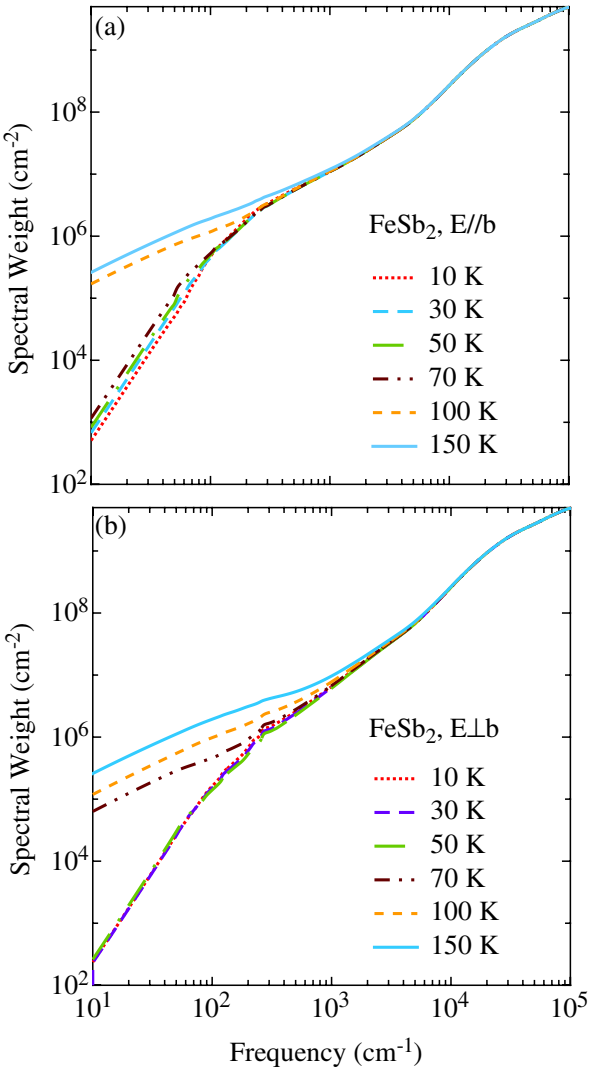

Fig. 6. (Color online) Integrated spectral weight as a function of temperature for light polarized along (a) and perpendicular (b) to the b crystallographic axis.

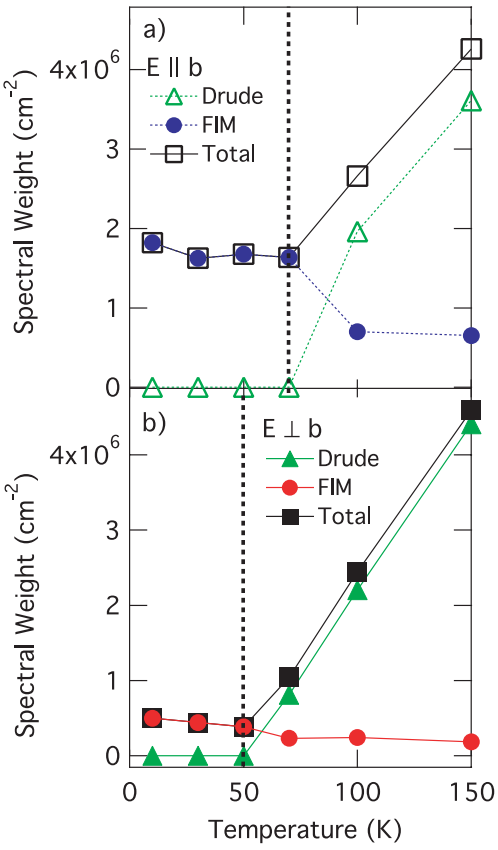

Fig. 7. (Color online) Temperature dependence of the spectral weight encountered in $\sigma_1(\omega)$ at $\omega < E_g$ for $E \parallel b$ (a) and $E \perp b$ (b). The dashed lines in (a) and (b) indicate the lower limit of $T_{MI}^{\parallel b}$ and $T_{MI}^{\perp b}$, respectively. The black squares represent the integrals of $\sigma_1(\omega)$ up to 300 cm^{-1} after having subtracted the fit to the phonon modes. The green triangles represent the spectral weight of the metallic Drude term. The blue and red circles represent the spectral weight (δA) of the broad infrared mode (FIM) for $E \parallel b$ and $E \perp b$, respectively.

300 cm^{-1}, which confirm our previous estimation of E_g. The overall depletion of $\sigma_1(\omega)$ at 10 K leads to a removal of spectral weight at low frequencies. The great majority of the suppressed spectral weight piles up in the spectral range between E_g and 3000 cm^{-1}. However, a full recovery of the spectral weight only occurs when integrating $\sigma_1(\omega)$ above 1 eV. The observation, that one needs to go to unusually high frequency to satisfy the conduction sum rule, might suggest, similarly to FeSi (Ref. [6]), that the physics of $FeSb_2$ involves an energy scale much larger than the gap energy E_g. The transfer of spectral weight in spectroscopies of correlated electron systems has been discussed in the framework of the periodic Anderson model for the situation pertinent to the Kondo insulators [25]. This latter model captures indeed some of the experimental findings; particularly, the apparent violation of the spectral weight sum rule when measuring at temperatures smaller than the size of the gap and restricted to a finite low frequency range.

We can now calculate how the total spectral weight encountered in $\sigma_1(\omega)$ of $FeSb_2$ at frequencies lower than E_g is redistributed. To do so we have first subtracted the phonons' contribution from the total weight. The temperature dependence of the total weight is plotted in Figure 7 for both polarization directions (open and filled black squares for $E \parallel b$ and $E \perp b$, respectively). We remark that at $T > T_{MI}$ a fraction of the total spectral weight below E_g is due to a background of weight distributed over an interval of energies extending from 0 up to E_g. We associate such a background to the presence of a continuum of low lying excitations. This continuum of excitations defines a broad far infrared mode (FIM). The total spectral weight up to E_g decreases with decreasing temperature down to T_{MI} (Fig. 7). Below T_{MI}, some residual spectral weight (which can not be of purely vibrational origin) survives inside of the gap. As demonstrated in Figure 7, the

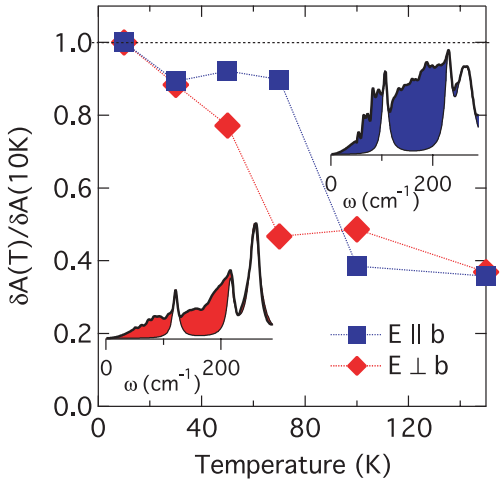

Fig. 8. (Color online) Temperature dependence of the normalized spectral weight (δA) of FIM. Insets show the area δA (blue and red for $E \parallel b$ and $E \perp b$, respectively) at low temperature, encountering the spectral weight of FIM (see text).

spectral weight of the Drude term disappears below T_{MI}. The removed Drude weight is transferred to high energies and partially piles up in the spectral range covered by FIM. The size of this FIM term increases indeed with decreasing temperature, as shown in Figure 7. The continuum of excitations, defining FIM, is better highlighted in the insets to Figure 8. The red and blue area for $E \parallel b$ and $E \perp b$, respectively, represent the spectral weight encountered in FIM (for the data at 10 K). Such areas (δA) are calculated by subtracting the spectral weight encountered in the Drude-Lorentz fit from the total spectral weight underneath the measured $\sigma_1(\omega)$ curve. Figure 8 displays then the temperature dependence of δA, normalized by its value at 10 K (Ref. [26]). At approximately T_{MI} the spectral weight associated to FIM suddenly increases and the T-dependence δA vaguely mimics the behaviour of an order parameter.

The temperature dependence of δA seems to shape the intrinsic electronic properties of $FeSb_2$. In fact, the presence of such a (FIM) continuum implies that several localized states are present at low temperatures between the valence and the conduction band. Above T_{MI} those states, generating FIM, are thermally occupied. Envisaging an overlapping of these states, a coherent electronic transport can then develop [1,2,27]. In this context, it is not surprising that T_{MI} is lower than E_g. Furthermore, the presence of this continuum of excitations supplies a natural explanation for the Fano behavior of the mode at $\omega_{03} = 261$ cm^{-1} for $E \perp b$. As anticipated above, the negative sign of the q Fano parameter implies an interaction of the mode at ω_{03} with a continuum covering an energy spectral range located below ω_{03}. Such a continuum of excitations is precisely provided by FIM. As comparison, we note that in the case of FeSi, where no evidence for an equivalent FIM feature was found, the asymmetry of the phonons was on the contrary ascribed to the red-shift of the gap edge [24]. The gap edge in $FeSb_2$ (see arrow in Figs. 2 and 3) does not display any clear red-shift with increasing temperature. Therefore, this excludes any possibility for a temperature dependent coupling between the phonon modes and mid infrared excitations.

One might speculate that, the states forming FIM might eventually be due to extrinsic, unintentional, dopants which provide local modes within the gap. This is, in our opinion, highly unlikely, since the resistivity grows by four to five orders of magnitude below T_{cr} and the contribution of defects in the dc transport barely leads to a modest change of the slope of $\rho(T)$ at low temperatures (inset of Fig. 3 in Ref. [1]). Extrinsic dopants [28] would, furthermore, show up in the tail of susceptibility (as it was discussed sometimes for FeSi). In $FeSb_2$ the impurity tail is very small and it develops only below 5 K (inset of Fig. 2 in Ref. [1]). Consequently, FIM is the new and most surprising feature in our spectra, which does not have any counterpart in FeSi and is not yet explained within the Kondo insulator approach [25].

4 Conclusion

The electrodynamic response of $FeSb_2$ is characterized by a metal-insulator crossover, occurring at $T < 70$ K and opening a gap $E_g \sim 300$ cm^{-1}. The depletion of $\sigma_1(\omega)$, due to the gap opening with decreasing temperature, signals the removal of spectral weight, which is shifted to energies higher than 1 eV. Furthermore, we have observed that the suppressed Drude weight at $T < T_{cr}$ partially piles up in the broad far infrared mode (FIM), which we have ascribed to a continuum of excitations. An ordinary semiconductor picture cannot account for the charge dynamics of $FeSb_2$. While some features in the optical response may be compatible with a Kondo insulator scenario, it remains to be seen how the presence of the continuum of excitations in the far infrared and at $\omega < E_g$ might eventually be consistent with such a description. In this respect, our findings could be a challenge for the theoretical treatment of the Kondo insulators within the framework of the periodic Anderson model [25]. Indeed, the effect of the lattice dynamics (e.g., through the formation of polaronic states) with respect to the spectral weight distribution has not been taken into account so far in the periodic Anderson model. Yet unexplored from the theoretical point of view is the possibility that the removed spectral weight might be also partially redistributed within the gap.

The authors wish to thank J. Müller for technical help, and G. Caimi, V. Dobrosavljevic, M. Ortolani, Z. Fisk and P.C. Canfield for fruitful discussions. This work has been supported by the Swiss National Foundation for the Scientific Research, within the NCCR research pool MaNEP and by the Office of Basic Energy Sciences of the US Department of Energy and it was partly carried out at the Brookhaven National Laboratory, which is operated for the US Department of Energy by Brookhaven Science Associates (DE-Ac02-98CH10886).

References

1. C. Petrovic, J.W. Kim, S.L. Bud'ko, A.I. Goldman, P.C. Canfield, W. Choe, G.J. Miller, Phys. Rev. B **67**, 155205 (2003)
2. C. Petrovic, Y. Lee, T. Vogt, N.Dj. Lazarov, S.L. Bud'ko, P.C. Canfield, Phys. Rev. B **72**, 045103 (2005)
3. V. Jaccarino, G.K. Wertheim, J.H. Wernick, L.R. Walker, S. Arajs, Phys. Rev. **160**, 476 (1967)
4. D. Mandrus, J.L. Sarrao, A. Migliori, J.D. Thompson, Z. Fisk, Phys. Rev. B **51**, 4763 (1995)
5. G. Aeppli, Z. Fisk, Comments Cond. Mat. Phys. **16**, 155 (1992)
6. Z. Schlesinger, Z. Fisk, H.-T. Zhang, M.B. Maple, J.F. DiTusa, G. Aeppli, Phys. Rev. Lett. **71**, 1748 (1993)
7. L. Degiorgi, M.B. Hunt, H.R. Ott, M. Dressel, B.J. Feenstra, G. Gruner, Z. Fisk, P.C. Canfield, Eur. Phys. Lett. **28**, 341 (1994)
8. M.A. Chernikov, L. Degiorgi, E. Felder, S. Paschen, A.D. Bianchi, H.R. Ott, J.L. Sarrao, Z. Fisk, D. Mandrus, Phys. Rev. B **56**, 1366 (1997)
9. S. Paschen, E. Felder, M.A. Chernikov, L. Degiorgi, H. Schwer, H.R. Ott, D.P. Young, J.L. Sarrao, Z. Fisk, Phys. Rev. B **56**, 12916 (1997)
10. A. Damascelli, Ph. D. thesis, University of Groningen, The Netherlands (1999)
11. F.P. Mena, J.F. DiTusa, D. van der Marel, G. Aeppli, D.P. Young, C. Presura, A. Damascelli, J.A. Mydosh, e-print `arXiv:cond-mat/0410481`
12. V.I. Anisimov, J. Zaanen, O.K. Andersen, Phys. Rev. B **44**, 943 (1991)
13. V.I. Anisimov, S.Y. Ezhov, I.S. Elfimov, I.V. Solovyev, T.M. Rice, Phys. Rev. Lett. **76**, 1735 (1996)
14. F. Wooten, in *Optical Properties of Solids* (Academic Press, New York, 1972)
15. M. Dressel, G. Grüner, in *Electrodynamics of Solids* (Cambridge University Press, 2002)
16. If we would force the measured $R(\omega)$ spectra at 50 and 70 K to a Hagen-Rubens extrapolation, a tiny residual Drude weight builds up in σ_1 below about 50 cm^{-1}, leaving however the spectra above 50 cm^{-1} totally unaffected.
17. The $R(\omega)$ spectra in the energy interval from 30 to 80 cm^{-1} above 70 K for $E \perp b$ and above 100 K for $E \parallel b$ (i.e., displaying a metallic behaviour) were interpolated with the $R(\omega)$ values calculated within the Hagen-Rubens extrapolation. This merging procedure between real data and extrapolation leads to a modest smoothing of the experimental data in the limited spectral range between 50 and 80 cm^{-1}. Furthermore, this merging procedure also results in a weak and artificial bump around 70 cm^{-1} in the $\sigma_1(\omega)$ spectra (Figs. 2–4), obtained through the Kramers-Kronig transformation.
18. P. Calvani, Riv. Nuovo Cimento **24**, 1 (2001)
19. U. Fano, Phys. Rev. **124**, 1866 (1961)
20. A. Damascelli, D. van der Marel, M. Grüninger, C. Presura, T.T.M. Palstra, J. Jegoudez, A. Revcolevschi, Phys. Rev. Lett. **81**, 918 (1998)
21. The broad ranges of T_{MI} are also compatible with the broad minimum of $\rho_{dc}(T)$ at T_{cr}, defining the MI transition in the temperature range between 40 and 80 K.
22. W.G. Fateley, F.R. Dollish, N.T. McDevitt, F.F. Bentley, in *Infrared and Raman Selection Rules for Molecular and Lattice Vibrations: The Correlation Method* (Wiley-Interscience, New York, 1972)
23. Along the direction perpendicular to the b axis (Fig. 4b), we can observe an additional feature centered at about 170 cm^{-1}. Its origin is at present uncertain. This feature is anomalously broad, such that its origin as phonon mode is quite unlikely.
24. A. Damascelli, K. Schulte, D. van der Marel, A.A. Menovsky, Phys. Rev. B **55**, R4863 (1997)
25. M.J. Rozenberg, G. Kotliar, H. Kajueter, Phys. Rev. B **54**, 8452 (1996)
26. The purpose of the normalized representation of δA in Figure 8 is to better emphasize the T-dependence of the FIM spectral weight, already shown in Figure 7, and to stress the possible order parameter behaviour of this quantity.
27. J.B. Goodenough, J. Solid State Chem. **5**, 144 (1972)
28. Single crystal X-ray diffraction measurement showed that the site occupancy does not deviate from an ideal $FeSb_2$ stoichiometry to within the resolution limit of 1% (Ref. [1]).